TECHNICAL MEMORANDUM

750

A parameterization of cloud overlap as a function of wind shear and its impact in ECMWF forecast

Francesca Di Giuseppe [1] and Adrian M. Tompkins[2]

[1]European Centre for Medium-Range Weather Forecasts, Reading, UK
[2]Abdus Salam International Centre for Theoretical Physics (ICTP), Trieste, Italy

Research Department

Abstract

Six months of CloudSat and CALIPSO observations have been divided into over eight million cloud scenes and co-located with ECMWF wind analyses to identify an empirical relationship between cloud overlap and wind shear for use in atmospheric models. For vertically continuous cloudy layers, cloud decorrelates from maximum towards random overlap as the layer separation distance increases, and we demonstrate a systematic impact of wind shear on the resulting decorrelation length scale. As expected, cloud decorrelates over smaller distances as wind shear increases. A simple, empirical linear fit parameterization is suggested that is straightforward to add to existing radiation schemes, although it is shown that the parameters are quite sensitive to the processing details of the cloud mask data and also to the fitting method used. The wind shear-overlap dependency is implemented in the radiation scheme of the ECMWF integrated forecast system. It has a similar magnitude impact on the radiative budget as that of switching from a fixed decorrelation length scale to the latitude-dependent length scale presently used in the operational model, altering the zonal mean, top-of-atmosphere, equator-to-mid latitude gradient of short-wave radiation by approximately 2 W m^{-2}.

1 Motivation

The representation of the vertical overlap of the cloud cover present in each grid cell of climate and numerical weather forecast models is key for their radiative transfer calculations. Some early models adopted one of two contrasting approaches, considering clouds to be either maximally (MAX) overlapped or randomly (RAN) overlapped (Geleyn and Hollingsworth (1979); Morcrette and Fouquart (1986)). Physical arguments soon lead to the suggestion to combine these to give the maximum-random (MAX-RAN) overlap scheme (Geleyn and Hollingsworth (1979)). This assumes that clouds present in adjacent vertical levels belong to a single coherent cloud system and thus are maximally overlapped, in contrast to clouds separated by clear layers which are randomly correlated.

The issue of cloud overlap assumptions were revisited by Hogan and Illingworth (2000), who used retrieval data from the Chilbolton radar in the UK. While the data confirmed that clouds separated by clear layers appeared randomly correlated (later corroborated in the analysis of ARM site data by Mace and Benson-Troth (2002)), the analysis revealed that vertically continuous cloudy layers decorrelated in height and that the maximum overlap assumption could thus underestimate cloud fraction in deep cloud systems. Hogan and Illingworth (2000) calculated the exponential decorrelation length scale, $\mathscr{L}$, for *continuous* clouds to be 2 km. The substitution of the MAX overlap assumption with an exponential decorrelation length scale lead Tompkins and Di Giuseppe (2007) to name this approach the EXP-RAN scheme.

Since the publication of Hogan and Illingworth (2000), a number of other studies using both ground-based observations have confirmed their findings. Willén et al. (2005) found a similar value of Hogan and Illingworth (2000) for a nearby ground station in Holland, while Mace and Benson-Troth (2002) reported a wide range of decorrelation length scales related to location and season, ranging from less than 1km to greater than 8km. Naud et al. (2008) also reported the impact of the dynamical situation and the season on the overlap statistics and decorrelation length scales, while confirming the validity of the EXP-RAN approach, and Oreopoulos and Norris (2011) also highlighted differences in cloud overlap between summer and winter seasons.

In addition to ground based information, the 94-GHz Cloud Profiling Radar (CPR) of CloudSat, which flies in the "A-Train" constellation of satellites with 1.30/13.30 equatorial crossing times and a return period of 16 days (Stephens et al. (2008)), provides global observations of the vertical structure of clouds, particularly when combined with CALIPSO lidar data to improve detection of thin cirrus clouds. Using

a different methodology that amalgamated both continuous and non-continuous cloud layers, Barker (2008) used two months of cloud mask data derived from CloudSat-CALIPSO satellite measurements and found a decorrelation lengthscale that varied as a function of latitude, but with a mean global value of 2 km. Cloud overlap was also examined in the CloudSat-CALIPSO dataset by Mace et al. (2009) who confirmed the model of EXP-RAN, and reported larger decorrelation length scales in the tropics where vertical velocities are high and wind shear is weaker.

In summary, a number of studies, using ground-based or satellite cloud observations have demonstrated that the EXP-RAN approach appears to be valid. They have reported a range of cloud decorrelation length scales for continuous cloudy columns and documented inter-location and inter-seasonal variations in this length scale. The variations have been attributed to changes in dynamics and stability, for example, whether cloud structures are dominated by convective conditions or the passage of mesoscale frontal systems (Naud et al. (2008)), which are associated with different vertical velocities and wind shears. Higher vertical velocity cloud systems will decorrelate less for a given wind shear. Likewise, clouds with small pristine ice crystals with low sedimentation rates will also decorrelate more for a given wind shear. In addition, Tompkins and Di Giuseppe (2015) shows that some of these differences can be attributed to the assumptions used to calculate the cloud overlap statistics themselves, and that decorrelation length scales are underestimated when sampled at spatial scales that are smaller than the typical cloud system scale. The findings of Tompkins and Di Giuseppe (2015) are very relevant for this work and the heuristic argument that data truncation could potentially lead to negative biases in the diagnosed α at larger cloud separations is explained in appendix A[1].

In this work, we focus on the basic impact of wind shear on the decorrelation of cloud systems. Hogan and Illingworth (2003) documented the impact of shear on ice clouds using ground based data in southern England and Lin and Mapes (2004) studied how wind shear impacts cloud-radiation feedback in the western Pacific warm pool. Naud et al. (2008) also conditionally sampled cloud overlap as a function of weak and strong wind shear and found only a limited impact. In their recent analysis of four years of CloudSat and CALIPSO measurements, Li et al. (2015) concluded that a statistical parameterization for the impact of dynamics including wind shear on cloud overlap would be beneficial for numerical models. Here we employ six months of CloudSat and CALIPSO data to study cloud overlap statistics in conjunction with co-located ECMWF wind analysis data and identify a simple empirical relationship between cloud overlap and wind shear that can be applied to atmospheric models.

The new parameterization is implemented in ECMWF cycle CY41R1 to assess its impact on radiative budget calculations.

2 Methodology

2.1 data

CloudSat and CALIPSO data for the period of January-July 2008 are used. All data are available at approximately 240 m vertical resolution (interpolated to a regular vertical grid) and 1.1 km horizontal resolution (Marchand et al. (2008)). Three datasets are used which are summarized in table 1. A first cloud mask dataset based only on CloudSat data is created where a layer is flagged as cloudy imposing a threshold of 20 on CloudSat cloud mask (Stein et al. (2011); Tompkins and Adebiyi (2012)) (see Figure 1b), and referred to as dataset "CS".

---

[1]The interested reader should refer to the published Tompkins and Di Giuseppe (2015) paper for details

Table 1: Cloud masks derived from the available CloudSat (CS) and CALIPSO (C) datasets.

Dataset name	Level 3 Products used	Condition for cloud pixel used
CS	2B-GEOPROF (CPR-mask)	CPR-mask > 20
CS-C	2B-GEOPROF (CPR-mask)	CPR-mask > 20 OR CloudFraction > 99%
	2B-GEOPROF-LIDAR (CloudFraction)	
CS-C-nr	2B-GEOPROF (CPR-mask)	(CPR-mask > 20 OR CloudFraction > 99%)
	2B-GEOPROF-LIDAR (CloudFraction)	AND precip-liquid-water+precip-ice-water=0
	2C-RAIN-PROFILE (precip-liquid-water, precip-ice-water)	

The thin cirrus that are not detected by the CloudSat radar (Mace et al. (2009)) can be detected by combining CloudSat Radar data with CALIPSO's dual wavelength lidar data. The dataset Cloud Fraction provides the fraction of lidar volumes in a radar volume identified as containing hydrometeor (Mace (2007); Mace and Zhang (2014); Mace et al. (2009)). Following Barker (2008), a layer is flagged as cloudy either if identified as such by the CloudSat algorithm, or if the lidar identified cloud fraction exceeds 99%. This combined product is referred to as CloudSat-CALIPSO, which is abbreviated to CS-C.

A problem that has been frequently pointed out is that the CloudSat *CPR* radar detects precipitation in addition to cloud droplets. The faster fall speeds imply that vertical correlations for rain will be higher than for cloud droplets, biasing cloud overlap statistics towards maximum overlap (Mace et al. (2009)). However, filtering out rainfall from the CloudSat dataset is not straightforward. An algorithm was proposed by Barker (2008) in an attempt to remove precipitation below the melting level by setting cloud fraction to zero if cloud was detected in the lowest retrieval layers, which are likely to contain precipitation unless foggy conditions prevail. This simple approach would leave precipitation that is present above the melting layer (e.g. snow) and would remove cloud near the surface. Alternatively, CloudSat also provides level 3 products with profiles of precipitation liquid and ice water content (2C-RAIN-PROFILE) which are consistently derived from the CloudSat Profiling Radar reflectivity and a constraint on the path integrated attenuation of the radar beam (Lebsock and L'Ecuyer (2011); L'Ecuyer and Stephens (2002)). Here, these products are used to determine a precipitation mask and only levels where no precipitable water is detected are flagged as cloudy (following Haynes et al. (2009); Haynes and Stephens (2007)) and is referred to as CloudSat-CALIPSO-norain, abbreviated to CS-C-nr.

Results are presented using this latter dataset, CS-C-nr, as a baseline. The data processing has nevertheless been performed using all three retrieval datasets and discrepancies in the final suggested parameterization are reported to provide an indication of the uncertainties associated with the retrieval assumptions. Table 1 summarizes the datasets employed and processing assumptions made.

The wind information is derived by locating the 25km grid point of the ECMWF operational integrated forecast system (IFS) that contains each individual 1.1km column in the CloudSat overpass (the nearest neighbour method is used and no spatial interpolation applied). The vertical profile of zonal and meridional winds, u and v, from the closest 6 hourly analysis time is projected onto the satellite overpass track to and then averaged in the along-track direction for all columns in a CloudSat data segment (described below) to give $\mathcal{V}$, the scene-average, along-track horizontal wind. The wind shear $\frac{d\mathcal{V}}{dz}_{i,j}$ between layers i and j is then simply defined as $\frac{d\mathcal{V}}{dz}_{i,j} = (\mathcal{V}_j - \mathcal{V}_i)/\mathcal{D}_{i,j}$, where $\mathcal{D}_{i,j}$ is the layer separation distance. Note that variations in wind between the two layers are neglected, and it is the meridional wind that contributes mostly to the statistics implying that cross-track shear associated with jets contributes little to the statistics.

2.2 Analysis Method

Each CloudSat data file is divided into scene segments of horizontal length of 50 km. Previous analysis typically used averaging length scales on the order of 50 to 300km to simulate the grid box sizes presently used in global numerical weather predictions or regional climate models and Hogan and Illingworth (2000) reported a significant sensitivity to this chosen sampling length scale. We apply a relatively short sampling scale to avoid averaging out wind shear features. Tompkins and Di Giuseppe (2015) address some of the reasons for the previous sensitivity of the decorrelation length to the sampling scale and suggests a simple filter of rejecting layers with cloud cover > 0.5 to reduce the scene-length dependency of the cloud overlap statistics, which is applied here.

Figure 1a shows the orbits of 3 days of observations (1-3 July 2008) and the associated along-track cloud profile (Fig 1b). Individual cloud sub-scenes are shown in Fig 1, c1 and c2, along with the co-located wind profile. For each of the cloud scenes the vertical overlap between any two layers with cloud cover C_i and C_j is analyzed if both C_i and C_j exceed 1%. Non-adjacent layers are considered to belong to a *continuous* cloud block if all layers found between are also classified as cloudy. The existence of any clear (cloud-free) layers instead will classify the two layers as non-continuous cloud. The observed total cloud cover is simply the projection of the two layers' cloud mask, $C_{i,j}^{obs}$. The joint C_i and C_j total cloud cover in the assumption of maximum overlap is $C_{i,j}^{max} = max\{C_i; C_j\}$ while in the assumption of random overlap is $C_{i,j}^{ran} = C_i + C_j - C_i C_j$. As in Hogan and Illingworth (2000), the observed total cloud cover can be expressed as a linear combination of the cloud covers derived from the MAX and RAN overlap assumptions.

$$C_{i,j}^{obs} = \alpha C_{i,j}^{max} + (1 - \alpha) C_{i,j}^{ran} \tag{1}$$

where α is the overlap parameter and can be written as

$$\alpha = \frac{C_{i,j}^{obs} - C_{i,j}^{ran}}{C_{i,j}^{max} - C_{i,j}^{ran}}. \tag{2}$$

Two cloud layers which are maximally overlapped will have $\alpha = 1$, while they will have $\alpha = 0$ if they are randomly overlapped. α could assume negative values in case of minimum overlap. We note the relatively short scene length of 50 km combined with the CloudSat resolution of 1.1km implies that cloud fraction is resolved to the nearest 2% approximately, meaning that α is poorly resolved as $C_i \to 0$ or $C_i \to 1$ (although the latter case is precluded by the cloud cover filter).

For each of the layer pairs, α has been calculated as a function of the inter-layer separation distance, $\mathscr{D}$. No information is retained on the height of the two layers, only their separation is considered. Thus two cloud layers at the same separation distance but at different altitudes will populate the same statistic group. Once this dataset is created it is subsequently conditionally sampled as a function of the wind shear, $\frac{d\mathscr{V}}{dz}$, between the two layers.

Finally, the reduction of α as a function of the separation distance is modeled by assuming an exponential decay (Fig. 3) for each wind shear bin. The exponential function is chosen for the simplicity of being a single parameter function and for coherence with previous studies. The exponential decorrelation length, $\mathscr{L}$, is thus derived from the best fit function $\alpha = e^{-\mathscr{D}/\mathscr{L}}$. We note that the fitting methodology varies in the literature, with the analysis of Shonk et al. (2010) in particular applying the exponential fit only using the data from adjacent cloud layers. The drawback of this method is that attempting to derive an exponential decorrelation length scale which lies in the range of O(2-4 km), using points separated by 240 m (an order of magnitude smaller) will result in greater sensitivity to retrieval uncertainties, especially for cases of small cloud fraction. We therefore include a range of cloud separation distances
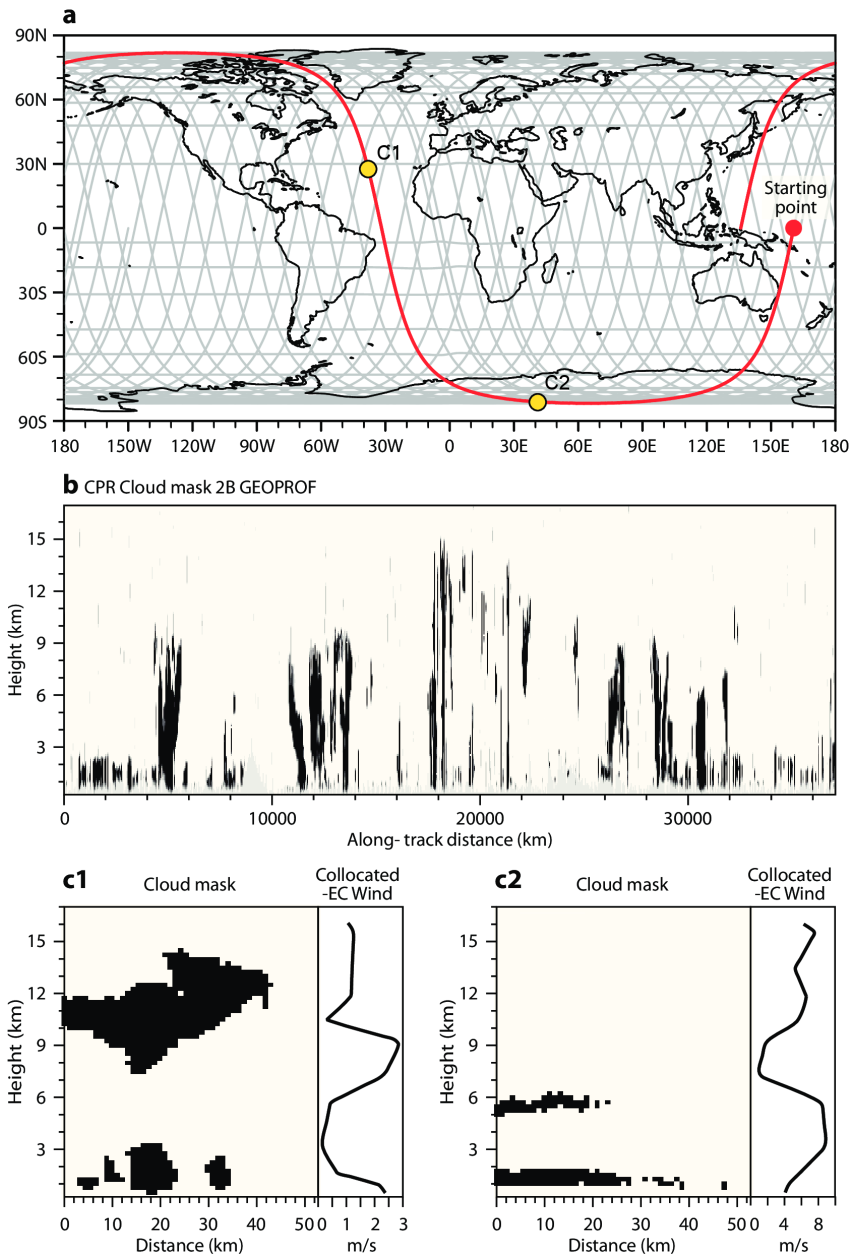
Figure 1: *(a) Map of CloudSat overpass tracks for 1-3 July 2008 marked in gray, (b) CloudSat cloud mask along the track highlighted in red in panel a, (c) Two 50km CloudSat sub-scenes from yellow point locations in panel a, along with the co-located wind profile from the ECMWF analysis*

when calculating the fit, and calculate $\mathscr{L}$ by least-squares fitting an exponential curve to the contiguous cloud layer α values. Two methods are applied, one in which all layer separations are included, provided at least 100 observations have contributed to the bin's statistics, and is referred to as "fit$_{all}$". In the second fitting method, a further restriction is applied that only layer separations up to 4 km are used (named fit$_{<4km}$).
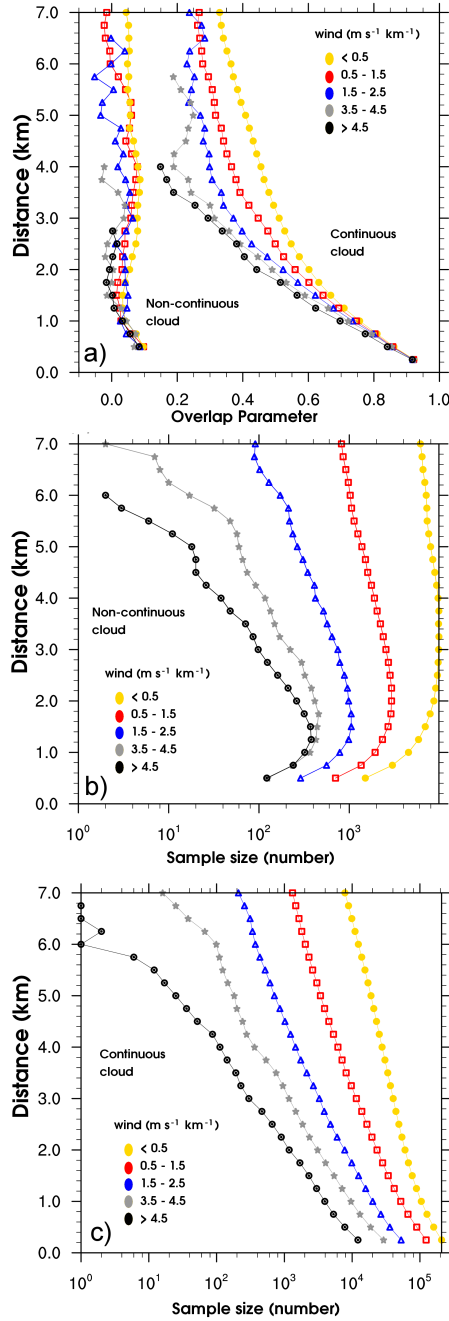
Figure 2:   a) Statistics from the six months of CloudSat and CALIPSO data processed using the Cs-C-nr algorithm. The overlap parameter, α, for sub-scenes of 50 km length, are divided into non-continuous and continuous cases, each of which are further divided into classes of vertical wind shear strength(only bins with at least 100 observations are shown). b) and c) panels; sample sizes for both continuous and non-continuous clouds.

2.3   Implementation into the ECMWF IFS radiation scheme

Tests are performed implementing the wind shear overlap parameterization derived in the paper into the short-wave and long-wave radiation schemes of latest cycle CY41R1 of ECMWF IFS.

The IFS radiation calculations are based on the Rapid Radiation Transfer Model (RRTM) of Mlawer et al. (1997) and Mlawer and Clough (1997) for the longwave and shortwave. The model implements the Monte-Carlo Independent Column Approximation (McICA) approach to handling overlap, whereby each g-point calculation of the radiation scheme is performed on a randomly-sampled column in which each layer is either cloud-free or overcast (Morcrette et al. (2008); Pincus et al. (2003); Räisänen et al. (2005)). The statistics of these sub-columns are such that, averaged over many sub-columns, the cloud fraction profile of the ECMWF grid column is obtained. Moreover, the total cloud cover of the columns corresponds to that of the imposed overlap scheme.

To generate the sub-columns, the algorithm of Räisänen et al. (2004) is employed. This algorithm implements the overlap assumption of Bergman and Rasch (2002), which is a pure EXP scheme, that is, the same exponential decorrelation length-scale is applied for both continuous and non-continuous cloudy columns, as also suggested by Barker (2008). This scheme will thus show greater sensitivity to the choice of $\mathscr{L}$ than the alternative EXP-RAN scheme of Hogan and Illingworth (2000), which instead assumes random overlap for layers separated by clear sky, but which is also cited by Räisänen et al. (2004) when referring to the overlap assumption used in the sampling algorithm.

The framework for testing the impact of the scheme is to integrate a lagged-start, 15-member ensemble of 24 hour forecasts using start dates from the 15th to the 30th of October 2009 at T_L95 horizontal resolution and with 91 vertical levels. Short forecast integrations are used in order to prevent the cloud structures from diverging from their initial conditions, and thus cloud-radiative impacts on the dynamics are largely precluded in these experiments. In addition to these short range forecasts the impact of the parameterization on the radiation is also evaluated in climate runs for a 4 member, lagged-start ensemble of 1 year uncoupled IFS integrations, using T_L255 (approximately 50km equivalent) horizontal resolution and 137 vertical layers.

The impact of the wind shear parameterization developed is bench marked against three alternative schemes for setting $\mathscr{L}$, outlined in table 2. In the first the $\mathscr{L}$ is simply fixed to an arbitrarily chosen decorrelation length scale of 3 km, referred to as experiment "Fix". The second method is the default option of IFS cycle CY41R1, which uses a latitude-dependent function (experiment "CY41R1"). This scheme was a minor modification to the original latitude-dependent scheme of Shonk et al. (2010), which is also used as a benchmark (experiment "Shonk"). The wind shear schemes are implemented in the same way as the existing parameterizations for $\mathscr{L}$; the scheme is applied to contiguous layers. As the wind shear parameterization derived later is linear, a minimum value of 0.5 km is applied to $\mathscr{L}$ to prevent unphysical negative values in (rare) high wind shear locations.

3   Results

3.1   Wind shear impact on cloud decorrelation

The cloud vertical decorrelation as a function of wind shear and distance is similar for the three datasets. Statistics are presented for the CS-C-nr dataset algorithm as an example. In the case of non-continuous cloud layers the assumption of random overlap is justified (Fig. 2a). The value of the overlap parameter,

Table 2: Summary of radiative calculation experiments where ϕ is the latitude in degrees and $\frac{d\mathcal{V}}{dz}$ represents wind shear ($m\,s^{-1}km^{-1}$).

Experiment	Description	$\mathcal{L}$ formulation (km)
Fix	Fixed value	$\mathcal{L} = 3$
Shonk	Latitude dependent scheme of Shonk et al. (2010)	$\mathcal{L} = 2.899 - 0.02759|\phi|$
CY41R1	Latitude dependent scheme of default Model	$\mathcal{L} = 0.75 + 2.149cos^2\phi$
Wind shear (Fit$_{all}$)	Wind shear fit to all layer separations	$\mathcal{L} = 5.2 - 0.60\frac{d\mathcal{V}}{dz}$
Wind shear (Fit$_{<4km}$)	Wind shear fit to layer separations<4 km	$\mathcal{L} = 4.4 - 0.45\frac{d\mathcal{V}}{dz}$

α, is less than 0.15 and is not strongly sensitive to layer separation and wind shear. Vertical continuous clouds are maximally overlapped at small separation distances, which is unsurprising, since by definition $C \to C^{max}$ as $\mathcal{D} \to 0$ as at zero separation one considers the overlap of a cloud with itself. The correlation reduces as layer separation distance increases (Fig. 2a). The different behavior of continuous and non-continuous cloud layers thus confirms the ground-based studies of Hogan and Illingworth (2000).

The least-squared exponential curves fitted using all data points of separations up to 4 km are given in Fig. 3. Comparing the curves to the original data in Fig. 2a, it is noted that the exponential curve appears a poor fit to the full range of separation distances, particularly in the cases of stronger wind shears. The exponential curve over-estimates the wind shear effect at small layer separations and under-estimates it at large separation distances. This implies that the value obtained for $\mathcal{L}$ will be sensitive to the conditions of the fitting method employed. The stronger wind shear cases occur orders of magnitude less frequently than weak wind shear categories, indicating that sampling may be an issue, (Fig. 2b,c). On the other hand, the fact that the variability in α is so limited for levels separated by small distances may be because the IFS analysis data is unlikely to resolve the differences in winds well at these small scales given its coarser temporal and spatial resolution. This is why both fitting methods use a range of separation distances and was also the motivation to use two fitting approaches to crudely assess $\mathcal{L}$ fitting uncertainty.

The decorrelation length-scales are given in table 3 as a function of cloud dataset, wind shear strength and exponential fitting method. The broad range of decorrelation values span those previously reported in the literature (e.g. Kato et al. (2010); Mace and Benson-Troth (2002); Naud et al. (2008); Oreopoulos et al. (2012); Oreopoulos and Norris (2011)), although no values are found under 2.5 km, greater than the values reported in Barker (2008); Hogan and Illingworth (2000). The first thing to note from table 3 is that there is considerable uncertainty in the derived values of $\mathcal{L}$ resulting from both the choice of dataset used for the analysis, and the fitting method itself. For example, using the first fitting method the length scale reduces from 5.1 to 4.3 km if the CS-C-nr dataset is used that attempts to filter out precipitation; an uncertainty of 15%. A similar uncertainty is also apparent resulting from the fitting method employed.

The table also shows a clear systematic impact of wind shear on the decorrelation length scale, with cloud decorrelating over smaller distances as wind shear increases. Again, the details of this relationship are sensitive to the fitting method employed, and it is clear from Fig. 2 that had only adjacent layers been employed to derive the fit, limited sensitivity to wind shear would have been reported. Even with very weak shear it is noted that cloud decorrelation occurs, likely due to a variety of causes. Firstly, the calculation of wind shear only accounts from the difference in wind between the two cloud layers, ignoring changes in wind between these layers and the impact of cross-track wind shear. Secondly the analysis of winds is subject to uncertainties, and also to a large extent represent the large-scale geostrophic flow, unless nearby sonde are available (e.g. Tompkins et al. (2005)). In addition, the 6 hourly temporal resolution of the analysis means that the wind profile may be up to 3 hours out of

Table 3: $\mathscr{L}$ (km) values from the exponential fit as a function of wind shear $\frac{d\mathscr{V}}{dz}$ (m $s^{-1}km^{-1}$), dataset (CS=CloudSat, CS-S=CloudSat-CALIPSO and CS-S-nr=CloudSat-CALIPSO-norain) and fitting method (Fit_{all} and $Fit_{<4km}$).

| $\frac{d\mathscr{V}}{dz}$ | Fit_{all} | | | $Fit_{<4km}$ | | |
	CS	CS-C	CS-C-nr	CS	CS-C	CS-C-nr
0.5	5.3	5.2	4.8	5.1	4.7	4.3
1.5	4.8	4.7	4.6	4.8	4.2	3.6
2.5	3.7	3.9	3.8	3.7	3.6	3.1
3.5	3.5	3.2	3.2	3.5	3.2	2.7
4.5	2.7	2.6	2.5	2.7	2.6	2.5

Table 4: Linear regression results of $\mathscr{L}$ (km) as a function of wind shear category $\frac{d\mathscr{V}}{dz}$ (m $s^{-1}km^{-1}$). Fit is $\mathscr{L} = \mathscr{L}_0 - \gamma\frac{d\mathscr{V}}{dz}$, where units of $\mathscr{L}_0$ are km.

| dataset | Fit_{all} | | | $Fit_{<4km}$ | | |
	L_0	γ	R^2	L_0	γ	R^2
CS	5.6	-0.65	0.97	5.5	-0.61	0.94
CS-C	5.6	-0.67	0.95	5.0	-0.52	0.95
CS-C-nr	5.2	-0.60	0.96	4.4	-0.45	0.94

synchronization with the CloudSat overpass.

The values of $\mathscr{L}$ only approach the 2 km reported by Hogan and Illingworth (2000) at strong wind shears. The study sites of Hogan and Illingworth (2000) was a mid-latitude where wind shears are stronger and cloud decorrelation is expected to be higher Shonk et al. (2010). It is also emphasized that the sensitivity to wind shear is likely to be underestimated here, due to the inability of the model analyses to resolve wind fluctuations on small spatial and temporal scales, and the fact that influence of cross-track wind shear values are neglected, which would include more extreme values associated with jet structures in the tropics and mid-latitudes.

Using the best-fit exponential decay length scale as a function of wind shear, $\frac{d\mathscr{V}}{dz}$, an empirical parameterization of $\mathscr{L}$ can be derived (Figure 4). A simple linear regression is suggested as

$$\mathscr{L} = \mathscr{L}_0 - \gamma\frac{d\mathscr{V}}{dz} \tag{3}$$

where γ and $\mathscr{L}_0$ are the fitting parameters and are reported in table 4 for all the three datasets and both fitting methods. The relationship is derived by performing a linear fit to the wind shear composite decorrelation length scale values. The value of $\mathscr{L}_0$ represents the extrapolation of $\mathscr{L}$ to exact zero wind shear. As the wind shear increases vertically continuous cloud layers decorrelate more rapidly with decorrelation length scales down to values of the order of 2 km.

3.2 Impact on ECMWF Integrated Forecasting System

3.3 Short-range forecast runs

The two wind shear related schemes are evaluated to assessed their impact relative to the implementation of latitude-dependent parameterizations for $\mathscr{L}$. The zonal averaged decorrelation length-scale as
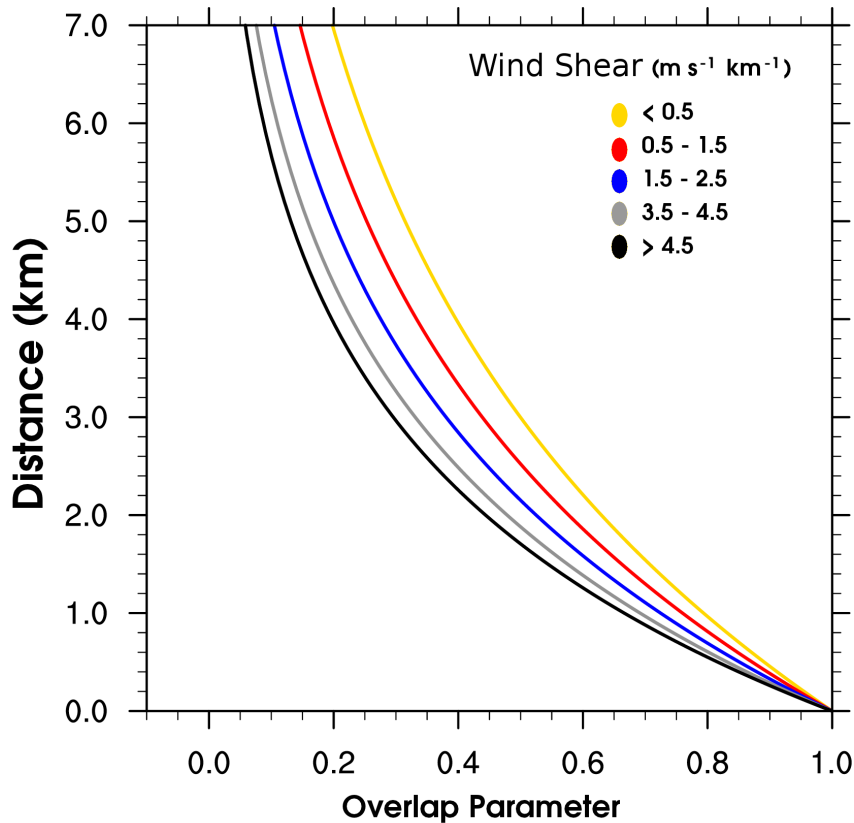
Figure 3: Parameterization for the continuous cloud overlap using the CloudSat-CALIPSO-norain (CS-C-nr) dataset. Best-fit exponential curves to the overlap parameter, α, for continuous cloud cases for each wind shear category.

a function of pressure or model level is given in Fig. 5. The Figure shows that $\mathscr{L}$ has higher values in the tropics, as expected due to the lower wind shear values there, with the exception of the upper troposphere due to the tropical easterly jet. Decorrelation of low level clouds in the boundary layer is also much higher. Zonal averaging masks the high variability in decorrelation length-scale that can reach values as low as the minimum imposed value of 0.5 km in high wind shear locations.

The impact of the spatially and temporally variable wind shear on the top of atmosphere fluxes also displays a latitude dependence (Fig. 6), with the weak wind shears in the tropics resulting in a high value of $\mathscr{L}$ and reduced total cloud cover with respect to the use of a fixed decorrelation value of 3 km. As a result the net SW radiation absorbed at the top of atmosphere (TOA) is increased by approximately 2 W m^{-2} using fitting method fit$_{all}$. The sign of the impact is the opposite of the two latitude-dependent (and very similar) schemes of Shonk et al. (2010) and CY41R1, which impose values for $\mathscr{L}$ similar to 3 km in the tropics, but which reduces at mid-latitudes. The magnitude of the impact of the wind shear scheme in terms of equator to mid-latitude differences is roughly similar in magnitude at 2 W m^{-2} for fit$_{all}$. Instead, using fitting method fit$_{<4km}$ reduces the impact on the radiation budget, as expected from the weaker wind shear dependency, by approximately 40%.
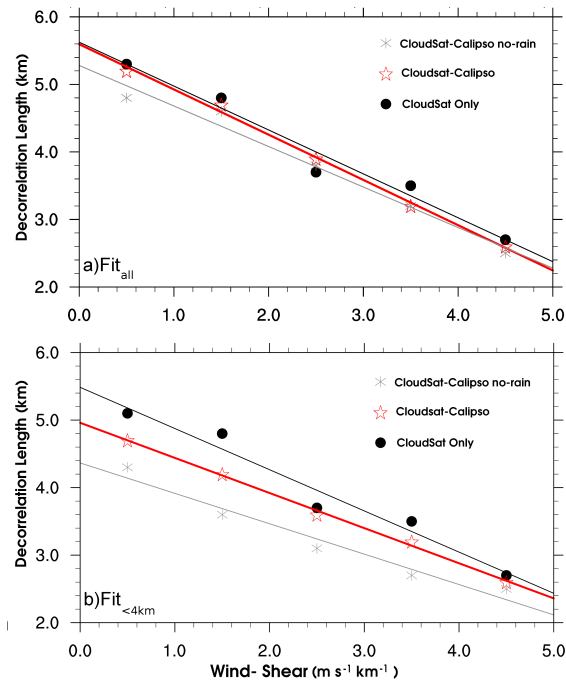
Figure 4: Decorrelation length scale from the best-fit exponential curves as a function of wind shear, with the straight lines giving the linear best-fit parameterization. The analysis has been repeated for the three datasets Cs, CS-C, and CS-C-nr and for (a) fit$_{all}$ and (b) fit$_{<4km}$. The discrepancies in the final suggested parameterization are reported to provide an indication of the uncertainties associated with the retrieval assumptions.
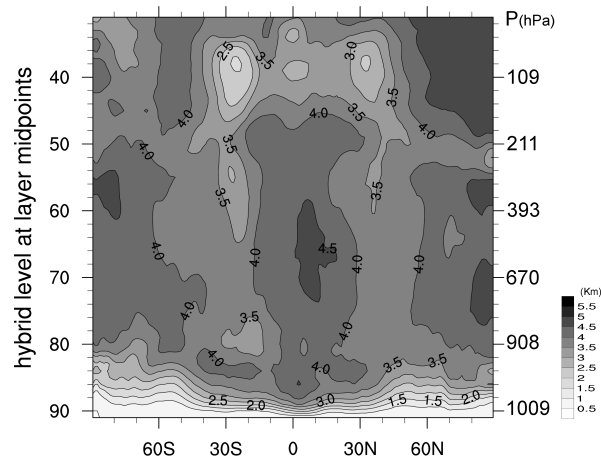

Figure 5: Zonal average of the decorrelation length value from experiment Wind shear (Fit$_{all}$).

3.4   Long-range forecast runs

A set of one year long integrations assess the impact of the new parameterization on the model climate. Even if the new parameterization does not introduce a systematic change in the diagnosed cloud cover the impact in long-range integrations is still noticeble when compared to the control experiment CY41R1 (figure 7).
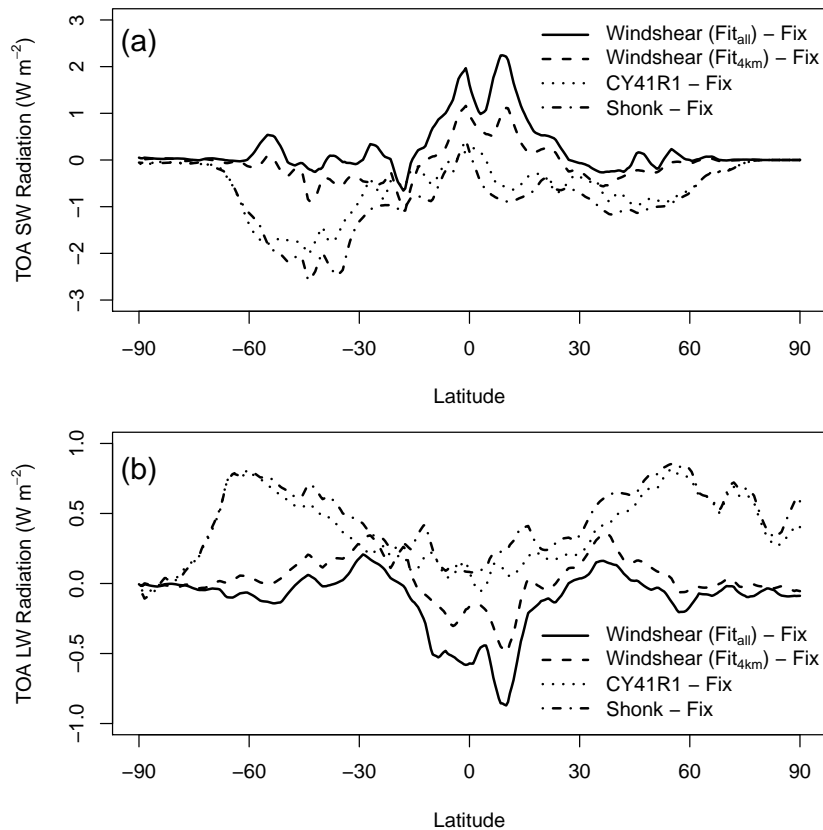
Figure 6: Zonal average differences of top of atmosphere (TOA) (a) shortwave (SW) and (b) longwave (LW) fluxes between the Shonk, CY41R1, wind shear parameterizations with respect to the fixed decorrelation lengthscale of 3 km (Fix), defined in the legend. Positive values indicate an increase in the downward direction.

Regions of high winds such as the extra-tropical to polar convey band where the jet-stream is active or the tropical trade wind tunnel is where the impact of the spatially and temporally variable wind shear parameterization is playing a major role on the top of atmosphere fluxes. Most of the impact is in the short wave. The control run comparison with observed longwave and shortwave top of the atmosphere radiation fluxes observed from CERES satellites shows that model shortwave radiation biases are mostly concentrated on the west coasts of continent due to the systematic overestimation of cloud thickness of the marine stratocumulus clouds in IFS (Duynkerke and Teixeira (2001)). The larger biases in the longwave outgoing radiations are located in the Sahel and they well document the southerly shift in the west-africa monsoon which is a persistent bias in many IFS releases (Di Giuseppe et al. (2013); Tompkins and Feudale (2010). Whatever the choice of the new parameterization implementation, the use of wind shear instead then a latitudinal dependency does not substantially reduce or modify the model climatic biases.

4   Discussion and Conclusions

This study has analyzed six months of CloudSat and CALIPSO data and confirmed that to a good ap-proximation clouds separated by clear sky gaps are randomly overlapped, while continuous cloud layers are close to maximally overlapped at small separations, but decorrelating with increasing layer separation
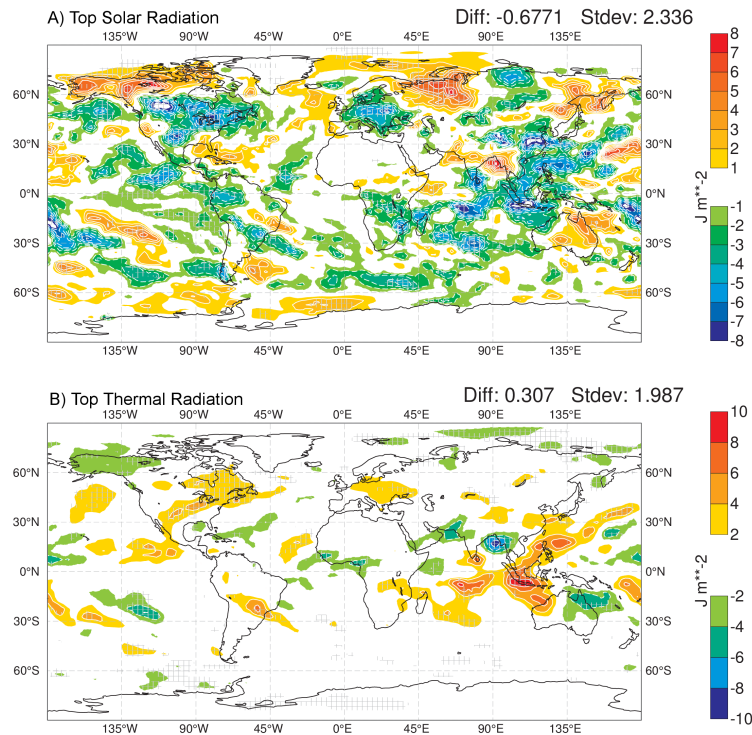
Figure 7: Panel a) Shortwave and panel b) Longwave top of the atmosphere radiation fluxes differences between the control run CY41R1 and the new wind shear based parameterization fit$_{<4km}$.

distance.

Focusing on the continuous cloudy layers, this study used co-located ECMWF wind profile analyses to composite these cases as a function wind shear, and found that the decorrelation length scale reduced with increasing wind shear as expected. The range of decorrelation values, when averaged over millions of combination, is between 5km and 2 km which is in overall agreement with the range of values reported in previous studies. A simple linear fit parameterization relating cloud decorrelation to wind shear is suggested that is straightforward to add to existing radiation schemes in atmospheric models using EXP or EXP-RAN schemes.

The new parameterization has been implemented in the ECMWF Integrated Forecasting System which uses the EXP overlap assumption, which assumes a single fixed decorrelation length scale for both continuous and non-continuous cloud layers, to assess its possible impact on the radiative budget calculations. The wind shear scheme is compared to the use of a fixed decorrelation length scale of 3 km and two experiments that implement a latitudinal dependency of $\mathcal{L}$. Relative to using a simple fixed decorrelation length scale of 3 km, the impact of the wind shear-dependent, decorrelation length scale was found to be similar to that of introducing the latitude-dependent scheme of Shonk et al. (2010).

We recall from the introduction that wind shear is just one factor that influences cloud overlap decorrelation, in addition to the analysis method, cloud dynamics in terms of updraft speeds and cloud ice microphysical properties that affect sedimentation rates (Heymsfield (1972)). These latter dynamical and microphysical effects are implicitly incorporated into the empirical latitude-dependent schemes of Shonk et al. (2010) and CY41R1 and it is thus emphasized that the comparison of decorrelation schemes performed in this work merely aims to gauge the impact of the wind shear specific parameterization relative to the use of a spatially variable latitude-dependent scheme, and not to suggest which of the
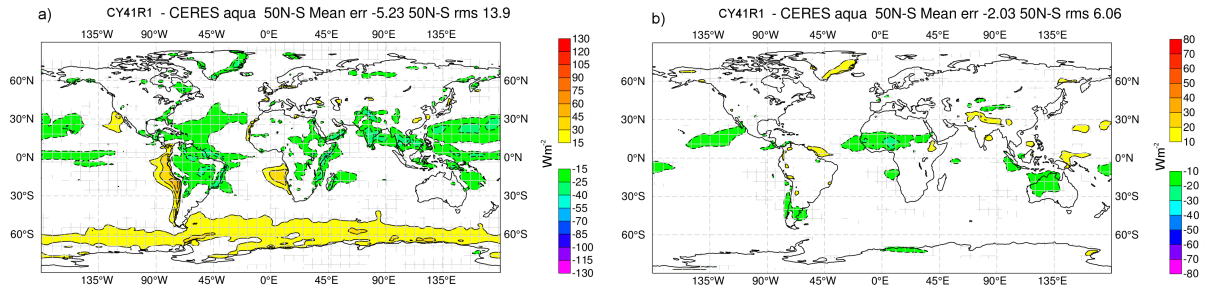
Figure 8: Panel a Shortwave and panel b Longwave top of the atmosphere radiation fluxes differences between the control run CY41R1 and CERES satellite observations.
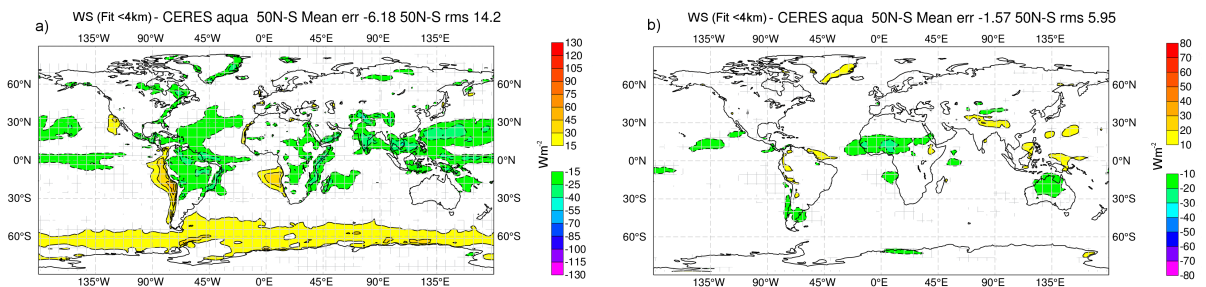

Figure 9: Same as figure 8 but for the new-parameterization implementation "fit$_{<4km}$"

schemes is superior. The next logical step would therefore be to use multi-variate statistical methodologies based on generalized linear models (Nelder and Baker (1972); Wolfinger and O'connell (1993)) to jointly derive the dynamical and spatial dependencies of the cloud decorrelation statistics.

A   Appendix: Sensitivity of the decorrelation length to the sampling scale

Tompkins and Di Giuseppe (2015) address some of the reasons for the previous sensitivity of the decorrelation length to the sampling scale and suggests a simple filter of rejecting layers with cloud cover > 0.5 to reduce the scene-length dependency of the cloud overlap statistics. In this appendix we will
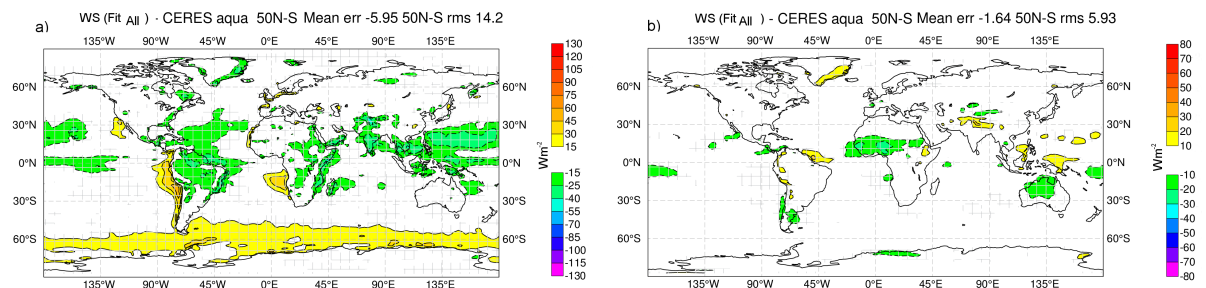

Figure 10: Same as figure 8 but for the new-parameterization with implementation "fit$_{all}$"

	Definition	Notes
X	Cloud system scale	Intrinsic dimension of the cloud system
X'	Sampling Scale	Sampling scale of the cloud scene. For Cloud-Sat data this refers to the scene length while in the case of a general circulatio model this refers to the grid resolution
$\frac{X'}{X}$	Sampling resolution	Ratio of the sampling to cloud system scale
α	Overlap parameter	Weight in the linear combination of the MAX ($\alpha = 1$) and RAN ($\alpha = 0$) overlap assumptions
$\mathscr{L}$	Decorreletion length scale	e-folding decay length scale of α for continuous clouds

provide a simple heuristic argument to justify this choice. The interested reader can refer to Tompkins and Di Giuseppe (2015) for a more detailed assessment of the problem.

The studies of Hogan and Illingworth (2000); Mace and Benson-Troth (2002); Naud et al. (2008); Oreopoulos and Norris (2011) showed a considerable sensitivity to the scene length chosen for the analysis, with decorrelation length-scale increasing with scene length. Mace and Benson-Troth (2002) and Hogan and Illingworth (2000) offered simple arguments to explain this based on a single cloud element, Mace and Benson-Troth (2002) also admitted that these arguments would likely not hold in real scenes where multiple cloud elements would need to be considered. Here, we will argue that the key short-coming of the consideration of Mace and Benson-Troth (2002) and Hogan and Illingworth (2000) is that the idealized cloud system they described was always fully contained within a scene and they did not consider the case when the sampling scale falls below the typical scale of cloud systems. In the following we will refer to the cloud system scale as X and the sampling scale (the length of the scenes into which a CloudSat data is divided for example) as X'. A summary of the symbols used in this appendix is reported in table A1.

As an example, Hogan and Illingworth (2000) state categorically that the degree of overlap must decrease monotonically with decreasing scene length. Consideration of the schematic in Fig. A1 shows that the assertion of Hogan and Illingworth (2000) does not necessarily hold once it falls below the cloud system scale, due to the issue of data truncation briefly discussed in Astin and Di Girolamo (2014). In the schematic, a simple cloud "system" of overlapping clouds close to maximum overlap is sampled at four sampling scales ($X' = A, B, C, D$).

At sampling scale $X' = A$ the whole cloud system is contained within a single scene. This is still the situation in example $X' = B$, even though the sampling scale is reduced. Comparing case A and B the argument of Hogan and Illingworth (2000) is correct; the cloud cover increases as the horizontal resolution increases and the degree of overlap reduces. However, in cases C and D the whole system is divided in two and three scenes, respectively. In case C, the division of the cloud system into two scenes results in maximal overlap in each. The situation is similar in case D, where the first and third segments are maximally overlapped, while the central segment is neglected as both layers are overcast. If either of the two scenes layers under consideration is overcast, the α parameter is undefined as all overlap assumptions give the same total cloud cover diagnosis of unity, and such scenes are neglected from the analysis. This is an example of the obvious effect of reducing the sampling scale, namely a
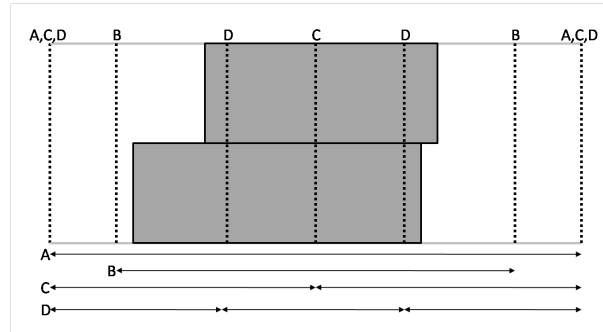
Figure A1: Schematic of the overlap of two adjacent clouds, shown with the gray block, which are sampled at four sampling scales (denoted A,B,C,D). The vertical dotted lines demark the scene boundaries, and the length of the scenes are indicated with the double headed arrows below the schematic for clarity.

greater proportional of the cloud layers will be overcast and rejected from the analysis (e.g. see the cloud fraction PDF derived from aircraft data over different sampling scales in Tompkins, 2003). Thus in this simple example, it is seen that the overlap decreases towards random while the cloud system is completely contained within a scene by the sampling scale chosen, but then increases to maximum overlap once the cloud system is divided into a number of separate scenes by a shorter sampling scale. In this case, α has a positive bias when the sampling scale X' is less than the cloud system scale X.

It is also possible to consider a two layer cloud, such as depicted in the example of Fig. A2, which is close to minimum overlap. For such cloud systems, in an arrangement where the extent of the cloud in each layer exceeds that of the overlapping portion and thus α is negative, it is clear that as X' reduces, only the scene that contains the overlapping portion will be considered. All other adjacent scenes contain cloud in only one layer and are thus ignored. Thus the overlapping portion of cloud sampled at small length-scales is minimally overlapped, leading to negative biases in this case.

Combining the above two cases, it appears that when alpha is negative, its sampling bias will be negative in the case of data truncation at small sampling scales, while positive α scenes will be subject to positive biases. To determine which, if any, of the two biases may dominate, we considering the limit of α as the sampling scale $X' \rightarrow 0$ for a minimally overlapped two layer system such as depicted in Fig.A2. As the sampling scale X' reduces, the cloud fraction in one layer will approach unity faster than the other [2]. If the cloud cover in the respective layers are C_1 and C_2, without loss of generality it is assumed that $C_1 > C_2$ so that $C_1 \rightarrow 1$ as X' reduces and that X' is sufficiently small such that the total cloud cover of the two layers is 1. The former condition implies $C_{1,2}^{max} = C_1$ and the overlap parameter derived for scene length X' can thus be written

$$\alpha(X') = \frac{1 - (C_1 + C_2 - C_1 C_2)}{C_1 - (C_1 + C_2 - C_1 C_2)} = 1 - \frac{1}{C_2}. \tag{1}$$

If the two cloudy layers are arranged in a configuration of minimum overlap, $C_2 \rightarrow 0$ as $X' \rightarrow 0$ and thus $\alpha(X') \rightarrow -\infty$. Thus α is unbounded for negative numbers but has an upper bound of 1. For minimal overlap cloud configurations with a finite overlap between the clouds, if $C_2 < 0.5$ as $C_1 \rightarrow 1$ then $\alpha(X') < -1$.

As a result of the assymmetry in the α bias, one can therefore expect that if a set of cloud systems that are randomly overlapped are sampled at length-scales shorter than the typical cloud system scale, that the negative bias due to scenes that contain cloud segments that are minimally overlapped will dominate

---

[2]the only possible, but unlikely, exception is if the cloud position in each layer is perfectly symmetrical.
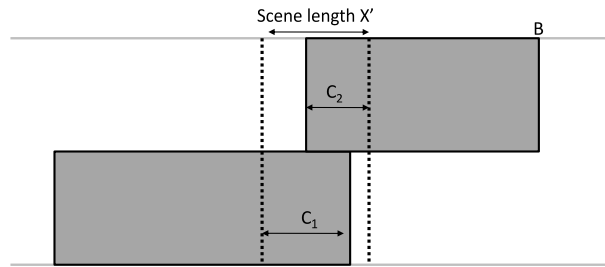
Figure A2: Schematic of the overlap of two adjacent clouds that are substantially minimally overlapped, showing that as the sampling scale X' reduces below the cloud-scale X, only the scene containing the overlapping portion will contribute to the derivation of the overlap parameter α.
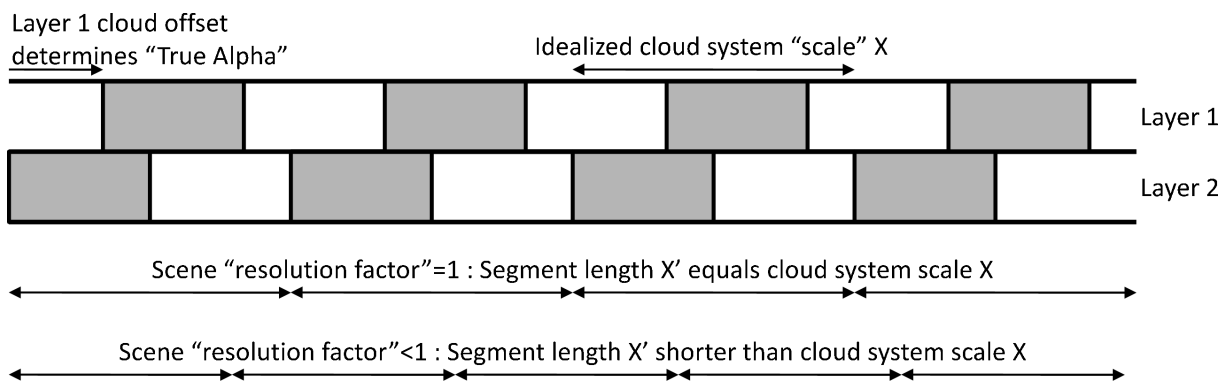

Figure A3: Schematic of the overlap of two adjacent clouds that form a plane parallel cloud system which repeats.

the positive bias occurring in sections that are close to be maximally overlapped. In these cases the mean value α will be negative as observed for discontinuous cloud layers reported in previous studies. Moreover, for continuous cloud layers the overlap at zero separation distance is unity by definition, but at larger separation distances the α value diagnosed will be more negative at shorter sampling scales. This would result in shorter decorrelation length-scale $\mathcal{L}$ being diagnosed.

We test this hypothesis in the the controlled framework of two layer cyclic clouds which are sampled at a range of sampling scales, as illustrated in Fig. A3. We consider a very simple cloud system that consists of a single cloud element of a fixed length $X/2$ that is repeated infinitely in the horizontal direction, with a spacing equal to the cloud length $X/2$. The simulated retrieval resolution is such that a scene of length X consists of $n = 100$ columns. The system is plane parallel and the system is repeated cyclically. Thus the cloud fraction measured at scales of nX, where $n \in Z$, is 50% in each scene. If the layer is sampled with scenes that are non-integer multiples of X other cloud fraction values are obtained in each segment. The length-scale X on which the cloud is period is referred to as the *cloud system scale*.

The cyclic cloud is repeated in a second layer, which can be offset (shifted) with respect to the first layer. If the offset is zero pixels then the cloud layers are maximally overlapped, while if the offset distance is $X/2$ the layers are minimally overlapped. Each possible overlap ranging from maximal to minimum is considered in turn, that is, in the first experiment the cloud layers are maximally overlapped, in the second experiment the cloud in layer 1 is shifted one column to the right, and so on until the layers are minimally overlapped, giving a total of $n/2 = 50$ experiments. In each experiment, the plane parallel scene is progressively sampled at decreasing *sampling scales*, X', starting at X and decreasing by one column at a time until the scene length is equal to $X/2$. We refer to the ratio X'/X as the *sampling resolution*.

The difference in the overlap parameter sampled at length X' and at the cloud system scale X provides the bias in α. We may not sample the clouds at scene length exceeding X due to the issue of aliasing when using periodically repeating cloud systems.

The results of this simple idealized case are shown in Fig. A4. By definition, if the sampling scale (X') is equal to the cloud system scale (X) and the sampling resolution is unity, the bias in α is identically zero. Panel (a) shows that as the sampling resolution X'/X decreases the bias of α can be of either sign depending on the value of α itself. If α lies between maximal ($\alpha = 1$) and random ($\alpha = 0$), or is even slightly minimally overlapped, its bias is positive. On the other hand, when the cloud system tends towards minimal overlapped, the bias becomes negative. However, it is also seen that the bias is highly nonlinear. The magnitude of the negative bias for scenes close to minimal overlap far exceeds the maximum positive bias found, confirming the arguments provided above.

If we now consider a set of cloud systems which, on average, are randomly overlapped, what would be the resulting sign of the bias at small sampling scales? Fig. A4a would appear to show that randomly overlapped clouds would be subject to a positive bias in α when the true α is zero. However, it is recalled that the overlap for a large set of observations is an average statistical property. For example, if we were to assume that discontinuous clouds are randomly overlapped, this does not imply that the total cover of any two cloud layers separated by a clear layer will be exactly random. Instead the overlap can take any value from maximum to minimum overlap, and the random overlap results from the averaging of many scenes. Indeed, for this idealized case of two layers of 50% cloud cover, all overlap possibilities from minimum through random to maximum would be equally likely.

Thus it is more appropriate to examine the mean overlap bias for all overlap cases that lead to the mean $\overline{\alpha}$, and we assume random overlap $\overline{\alpha}=0$ to be the mean for all overlap cases ranging from maximum overlap $\alpha=1$ to minimum $\alpha=-1$, while $\overline{\alpha}=0.5$ is the average for individual overlap cases ranging from maximum overlap ($\alpha=1$) to random ($\alpha=0$) for example. The averaged α bias calculation (Fig. A4b) appears to support the heuristic argument above and previous observational investigations of overlap can potentially be explained. Although the α bias is positive for a wider range of α values when the sampling resolution X'/X is less than unity, (for example, Fig. A4a shows that for $X'/X=0.6$, the bias is positive for α values exceeding ≈ -0.3), the larger magnitude of the negative bias in minimally overlapped clouds can dominate. This results in negative biases for $\alpha < 0.1 - 0.2$, depending on the sampling resolution. Thus clouds that are randomly overlapped would be diagnosed with a negative α values between up to -0.2 when using sampling resolutions between 0.5 and 1.0, based on this simple cyclic cloud system study. This range of negative α values is consistent with the values previous reported for discontinuous clouds, such as in the work of Naud et al. (2008), but were previous not explained. Here the hypothesis is therefore that that these scenes are, in fact, randomly overlapped, and the negative overlap parameter is result of the scene lengths used being less than the typical cloud system scale. In addition, the decorrelation length scale should reduce with higher resolution/shorter averaging periods as observed previously.
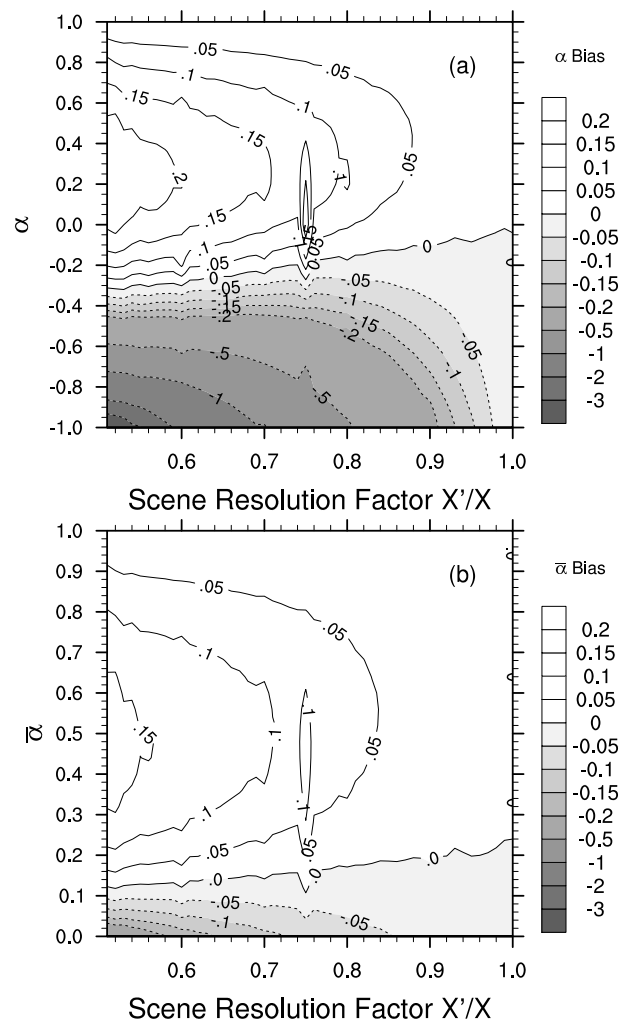
Figure A4: Results of the idealized cloud sampling test illustrated in fig. A3. (a) Bias in α as a function of the true overlap for individual cloud combinations and sampling length-scale. (b) Bias in α averaged over all cloud combinations that give $\overline{\alpha}$.

References

Astin, I., and L. Di Girolamo, 2014: Technical note: The horizontal scale-dependence of the cloud overlap parameter alpha. *Atmos. Chem. Phys. Dis.*, **14 (7)**, 9801–9813.

Barker, H. W., 2008: Overlap of fractional cloud for radiation calculations in GCMs: A global analysis using CloudSat and CALIPSO data. *J. Geophys. Res.*, **113**, DOI: 10.1029/2007JD009 677.

Bergman, J. W., and P. J. Rasch, 2002: Parameterizing vertically coherent cloud distributions. *J. Atmos. Sci.*, **59**, 2165–2182.

Di Giuseppe, F., F. Molteni, and E. Dutra, 2013: Real-time correction of ERA-Interim monthly rainfall. *Geophys. Res. Lett.*, **40 (14)**, 3750–3755.

Duynkerke, P. G., and J. Teixeira, 2001: Comparison of the ecmwf reanalysis with fire i observations: Diurnal variation of marine stratocumulus. *Journal of climate*, **14 (7)**, 1466–1478.

Geleyn, J. F., and A. Hollingsworth, 1979: An economical analytical method for the computation of the interaction between scattering and line absorption of radiation. *Contrib. Atmos. Phys*, **52**, 1–16.

Haynes, J. M., T. S. L'Ecuyer, G. L. Stephens, S. D. Miller, C. Mitrescu, N. B. Wood, and S. Tanelli, 2009: Rainfall retrieval over the ocean with spaceborne w-band radar. *Journal of Geophysical Research: Atmospheres (1984–2012)*, **114 (D8)**.

Haynes, J. M., and G. L. Stephens, 2007: Tropical oceanic cloudiness and the incidence of precipitation: Early results from CloudSat. *Geophys. Res. Lett.*, **34**, 9811.

Heymsfield, A., 1972: Ice crystal terminal velocities. *J. Atmos. Sci.*, **29 (7)**, 1348–1357.

Hogan, R. J., and A. J. Illingworth, 2000: Deriving cloud overlap statistics from radar. *Q. J. R. Meteorol. Soc.*, **126**, 2903–2909.

Hogan, R. J., and A. J. Illingworth, 2003: Parameterizing ice cloud inhomogeneity and the overlap of inhomogeneities using cloud radar data. *J. Atmos. Sci.*, **60**, 756–767.

Kato, S., S. Sun-Mack, W. F. Miller, F. G. Rose, Y. Chen, P. Minnis, and B. A. Wielicki, 2010: Relationships among cloud occurrence frequency, overlap, and effective thickness derived from CALIPSO and CloudSat merged cloud vertical profiles. **115 (D4)**, DOI: 10.1029/2009JD012 277.

Lebsock, M. D., and T. S. L'Ecuyer, 2011: The retrieval of warm rain from cloudsat. *J. Geophys. Res.*, **116 (D20)**, 10.1029/2011JD016 076.

L'Ecuyer, T. S., and G. L. Stephens, 2002: An estimation-based precipitation retrieval algorithm for attenuating radars. *J. Appl. Meteor.*, **41 (3)**, 272–285.

Li, J., J. Huang, K. Stamnes, T. Wang, Q. Lv, and H. Jin, 2015: A global survey of cloud overlap based on calipso and cloudsat measurements. *Atmos. Chem. Phys.*, **15 (1)**, 519–536.

Lin, J. L., and B. E. Mapes, 2004: Wind shear effects on cloud-radiation feedback in the western Pacific warm pool. *Geophys. Res. Lett.*, **31**, L16 118, doi:10.1029/2004GL020 199.

Mace, G. G., 2007: Level 2 GEOPROF product process description interface control document(V5.3). Tech. rep., CIRA, Colorado State University, CIRA, Colorado State University, available at http://www.cloudsat.cira.colostate.edu/ pp.

Mace, G. G., and S. Benson-Troth, 2002: Cloud-layer overlap characteristics derived from long-term cloud radar data. *J. Climate*, **15**, 2505–2515.

Mace, G. G., and Q. Zhang, 2014: The cloudsat radar-lidar geometrical profile product (rl-geoprof): Updates, improvements, and selected results. *Journal of Geophysical Research: Atmospheres*, **119 (15)**, 9441–9462.

Mace, G. G., Q. Zhang, M. Vaughan, R. Marchand, G. Stephens, C. Trepte, and D. Winker, 2009: A description of hydrometeor layer occurrence statistics derived from the first year of merged CloudSat and CALIPSO data. *J. Geophys. Res.*, **114**, DOI: 10.1029/2007JD009 755.

Marchand, R., G. G. Mace, T. Ackerman, and G. Stephens, 2008: Hydrometeor detection using cloudsat-an earth-orbiting 94-ghz cloud radar. *J. Atmos. Ocean. Tech.*, **25 (4)**, 519–533.

Mlawer, E. J., and S. Clough, 1997: Shortwave and longwave enhancements in the Rapid Radiative Transfer Model. *Proc. of the 7th Atmospheric Radiation Measurement (ARM) Science Team Meeting*, U.S. Department of Energy, available at http://www.arm.gov/publications, ARM, CONF–9603 149.

Mlawer, E. J., S. J. Taubman, P. D. Brown, M. J. Iacono, and S. A. Clough, 1997: Radiative transfer for inhomogeneous atmospheres: RRTM, a validated correlated-k model for the longwave. *J. Geophys. Res.*, **102**, 16 663–16 682.

Morcrette, J., H. Barker, J. Cole, M. Iacono, and R. Pincus, 2008: Impact of a new radiation package, mcrad, in the ecmwf integrated forecasting system. *Monthly Weather Review*, **136 (12)**, 4773–4798.

Morcrette, J.-J., and Y. Fouquart, 1986: The overlapping of cloud layers in shortwave radiation parameterizations. *J. Atmos. Sci.*, **43**, 321–328.

Naud, C. M., A. Del Genio, G. G. Mace, S. Benson, E. E. Clothiaux, and P. Kollias, 2008: Impact of dynamics and atmospheric state on cloud vertical overlap. *J. Climate*, **21 (8)**, 1758–1770.

Nelder, J. A., and R. Baker, 1972: Generalized linear models. *Encyclopedia of Statistical Sciences*.

Oreopoulos, L., D. Lee, Y. Sud, and M. Suarez, 2012: Radiative impacts of cloud heterogeneity and overlap in an atmospheric general circulation model. *Atmospheric Chemistry and Physics*, **12 (19)**, 9097–9111.

Oreopoulos, L., and P. Norris, 2011: An analysis of cloud overlap at a midlatitude atmospheric observation facility. *Atmospheric Chemistry and Physics*, **11 (12)**, 5557–5567.

Pincus, R., H. W. Barker, and J. J. Morcrette, 2003: A fast, flexible, approximate technique for computing radiative transfer in inhomogeneous cloud fields. *J. Geophys. Res.*, **108**, 10.1029/2002JD003 322.

Räisänen, P., H. W. Barker, and J. N. S. Cole, 2005: The Monte Carlo independent column approximation's conditional random noise: impact on simulated climate. *J. Climate*, **18**, 4715–4730.

Räisänen, P., H. W. Barker, M. F. Khairoutdinov, J. Li, and D. A. Randall, 2004: Stochastic generation of subgrid-scale cloudy columns for large-scale models. *Q. J. R. Meteorol. Soc.*, **130 (601)**, 2047–2067.

Shonk, J. K., R. J. Hogan, J. M. Edwards, and G. G. Mace, 2010: Effect of improving representation of horizontal and vertical cloud structure on the earth's global radiation budget. part i: Review and parametrization. *Quarterly Journal of the Royal Meteorological Society*, **136 (650)**, 1191–1204.

Stein, T. H. M., D. J. Parker, J. Delanoë, N. S. Dixon, R. J. Hogan, P. Knippertz, R. I. Maidment, and J. H. Marsham, 2011: The vertical cloud structure of the West African monsoon: A four-year climatology using CloudSat and CALIPSO. *J. Geophys. Res.*, **116**, doi:10.1029/2011JD016 029.

Stephens, G. L., and Coauthors, 2008: CloudSat mission: Performance and early science after the first year of operation. *J. Geophys. Res.*, **113**, doi:10.1029/2008JD009 982.

Tompkins, A. M., 2003: Impact of temperature and total water variability on cloud cover assessed using aircraft data. *Q. J. R. Meteorol. Soc.*, **129**, 2151–2170.

Tompkins, A. M., and A. A. Adebiyi, 2012: Using cloudsat cloud retrievals to differentiate satellite-derived rainfall products over west africa. *Journal of Hydrometeorology*, **13 (6)**, 1810–1816.

Tompkins, A. M., and F. Di Giuseppe, 2007: Generalizing cloud overlap treatment to include solar zenith angle effects on cloud geometry. *J. Atmos. Sci.*, **64**, 2116–2125.

Tompkins, A. M., and F. Di Giuseppe, 2015: An interpretation of cloud overlap statistics. *J. Atmos. Sci.*, **–**, in press.

Tompkins, A. M., A. Diongue, D. J. Parker, and C. D. Thorncroft, 2005: African easterly jet in the ECMWF integrated forecast system: 4D-Var analysis. *Q. J. R. Meteorol. Soc.*, **131**, 2861-2886.

Tompkins, A. M., and L. Feudale, 2010: West Africa monsoon seasonal precipitation forecasts in ECMWF System 3 with a focus on the AMMA SOP. *Wea. and Forecasting*, **25**, 768–788.

Willén, U., S. Crewell, H. K. Baltink, and O. Sievers, 2005: Assessing model predicted vertical cloud structure and cloud overlap with radar and lidar ceilometer observations for the baltex bridge campaign of cliwa-net. *Atmospheric research*, **75 (3)**, 227–255.

Wolfinger, R., and M. O'connell, 1993: Generalized linear mixed models a pseudo-likelihood approach. *J. Stat. Comput. Sim.*, **48 (3-4)**, 233–243.